Spectroscopic optical coherence tomography

U. Morgner, W. Drexler, F. X. Kärtner, X. D. Li, C. Pitris, E. P. Ippen, and J. G. Fujimoto

Department of Electrical Engineering and Computer Science and Research Laboratory of Electronics, Massachusetts Institute of Technology, Cambridge, Massachusetts 02139

Received August 2, 1999

Spectroscopic optical coherence tomography (OCT), an extension of conventional OCT, is demonstrated for performing cross-sectional tomographic and spectroscopic imaging. Information on the spectral content of backscattered light is obtained by detection and processing of the interferometric OCT signal. This method allows the spectrum of backscattered light to be measured over the entire available optical bandwidth simultaneously in a single measurement. Specific spectral features can be extracted by use of digital signal processing without changing the measurement apparatus. An ultrabroadband femtosecond Ti:Al_2O_3 laser was used to achieve spectroscopic imaging over the wavelength range from 650 to 1000 nm in a simple model as well as *in vivo* in the *Xenopus laevis* (African frog) tadpole. Multidimensional spectroscopic data are displayed by use of a novel hue-saturation false-color mapping. © 2000 Optical Society of America

OCIS codes: 110.4500, 100.6950, 100.7410.

Optical coherence tomography (OCT) has emerged as a promising medical diagnostic imaging technology for noninvasive *in situ* cross-sectional imaging of biological tissues and materials.[1] Recently, extensions of OCT technology, including Doppler flow[2,3] and polarization-sensitive[4,5] imaging, have been developed that permit spatially resolved imaging of velocity or birefringence. The axial resolution of OCT is determined by the bandwidth of the low-coherence light source, and image resolutions 10–100 times better than standard ultrasound imaging have been achieved. Ultrashort-pulse mode-locked Ti:Al_2O_3 laser technology has made it possible to generate pulses shorter than two optical cycles, corresponding to bandwidths of 350 nm, centered around 800 nm.[6] This laser is a powerful source for ultrahigh-resolution and spectroscopic OCT imaging. *In vivo* subcellular imaging in the *Xenopus laevis* tadpole has been demonstrated with 1 μm axial by 3 μm transverse resolution, what is to our knowledge the highest OCT resolution to date.[7]

In this Letter, we demonstrate broadband spectroscopic OCT, an extension of standard OCT technology. Spectroscopic and wavelength-dependent OCT is a new area of investigation, and few studies of it have been performed to date because sufficiently broadbandwidth light sources have not been available. One previous study demonstrated spectroscopic detection over a bandwidth of ~50 nm at 1.3 μm.[8] Other studies were performed at 1.3 and 1.5 μm, combining two separate light sources to detect water content in tissue.[9,10] By use of state of the art femtosecond Ti:Al_2O_3 lasers, spectroscopic information over the entire output bandwidth from 650 to 1000 nm can be obtained. This spectral region is important because it overlaps absorption features in oxyhemoglobin and deoxyhemoglobin and may permit the functional imaging of hemoglobin oxygen saturation. Spectroscopic OCT can also be used to enhance image contrast, permitting the differentiation of tissue pathologies through their spectroscopic properties or functional states. This spectroscopic staining is somewhat analogous to histological staining.

OCT uses interference of low-coherence (i.e., broadband) light in a Michelson interferometer. Light from a reference path with length $z = \nu_g \tau$, scanned continuously at a speed ν_g, is interfered with light from the sample. The beam position on the sample is scanned in the transverse x direction, creating a cross section through the object under study. By use of a broadband light source with a spectrum $|E(\omega)|^2$, the detected intensity at the output of the interferometer as a function of τ or z is given by

$$I_D(z) = \int |E(\omega) r_{\mathrm{BS}}(\omega) t_{\mathrm{BS}}(\omega) [\exp(ikz) + r_S(\omega, z)]|^2 D(\omega) \mathrm{d}\omega \,, \quad (1)$$

where k is the wave number, $D(\omega)$ is the detector response, and $r_S(\omega, z)$, $r_{\mathrm{BS}}(\omega)$, and $t_{\mathrm{BS}}(\omega)$ are the complex reflectivity of the sample and the reflectivity and transmissivity of the interferometer beam splitter, respectively. $I_D(\tau = z/\nu_g)$ is the oscillating output from interference of the signal field with the Doppler-shifted reference field. Figure 1 shows an example of data from a single axial scan. Each delay τ corresponds to detecting light that is backscattered from a corresponding depth z inside the tissue, whose depth resolution is given by the point spread function $P(\tau)$, where $P(\tau)$ is obtained from $I_D(\tau)$ for $r_S(\omega) = 1$ by Fourier transform F.

In standard OCT imaging, only the envelope of the interference signal $I_D(\tau)$ is detected. The OCT image is a two-dimensional array representing the backscattered intensity $T(x, z) = En\nu[I_D(z)]$. Spectral information can be obtained by measurement of the full interference signal and the use of appropriate digital signal processing. Spectroscopic detection is performed with a Morlet wavelet transform that reduces

0146-9592/00/020111-03$15.00/0

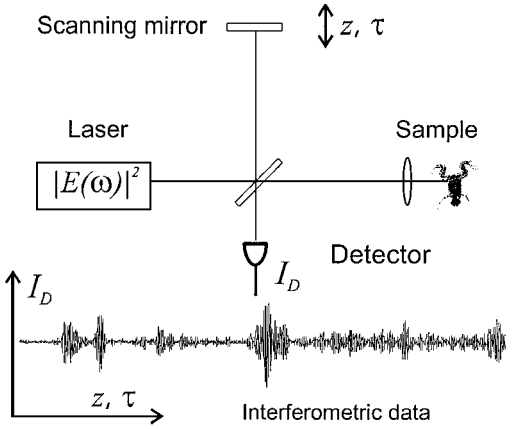

Fig. 1. OCT schematic. The broadband laser source is coupled into a Michelson-type interferometer. The resulting interferogram $I_D(\tau)$ contains spectroscopic information about the reflected–backscattered light. The envelope of $I_D(\tau)$ is used in standard OCT imaging to detect the intensity of the reflected–backscattered light.

windowing artifacts associated with other methods such as the short-time Fourier transform.[11] The Morlet wavelet transformation is given by

$$W(\Omega, \tau) = \left| \int I_D(t + \tau)\exp[-(t/t_0)^2]\exp(i\Omega t)\mathrm{d}t \right|^2$$

$$= |F\{I_D(t + \tau)\exp[-(t/t_0)^2]\}|^2. \quad (2)$$

The advantage of this technique is that an entire spectrum $W(\Omega)$ can be calculated for each point (x, τ) in the OCT image. For the purposes of demonstration, and to display the spectroscopic data in a simple color image, we calculated the center of mass $\Omega_C(x, z)$ of the spectra. It is also possible to extract spectroscopic information at a specific single frequency, within a given bandwidth, at multiple discrete wavelengths, etc. Unlike in standard OCT, displaying the spectroscopic OCT image requires a multidimensional map. Hue, saturation, luminance color space (not red-green-blue) was used to map the backscattering intensity $T(x, z)$ into the saturation and the spectral center of mass $\Omega_C(x, z)$ into the hue, keeping luminance constant. This approach permits the intensity and the spectral shift of the backscattered light to be visualized.

The experimental apparatus for spectroscopic OCT is similar to that for *in vivo* ultrahigh-resolution OCT. We used a high-speed (5-Msamples/s, 12-bit) analog–digital converter to digitize the interference signal, instead of measuring only the envelope as in conventional OCT. Dispersion and polarization were matched in the interferometer arms, and special fibers, a 3-dB splitter, lenses, signal filtering, and demodulation were used to support the broad optical and electronic bandwidths. A precision galvanometer was used to scan the reference arm, and nonlinearities in speed v_g were relatively small, so interferometric triggering methods were not required.

As a demonstration, spectroscopic OCT imaging was performed on a thin semiconductor-doped glass wedge (Schott RG-850) on top of a silver mirror (see Fig. 2). The colored glass absorbs short wavelengths and transmits infrared (cf. the transmission characteristics in the bottom part of Fig. 2). The light is focused on the silver mirror and passes through the color wedge twice. We performed spectroscopic OCT imaging by recording the interferometric signal $I_D(x, z)$ over 10,000 data points, at 1000 transverse positions, resulting in a 10-MB image size. The interferometric signal was processed with the wavelet transformation, and the center of mass of the reflected spectra was calculated and displayed. The resulting false-color hue-saturation image is shown in the top part of Fig. 2. The center of mass of the spectrum is mapped onto a red-green hue in the image. A green hue indicates a spectral shift to shorter wavelengths and a red hue, a shift to longer wavelengths, whereas yellow is neutral. At positions where the wedge is thicker, the spectrum of the backreflected light is shifted to longer wavelengths.

To demonstrate spectroscopic OCT *in vivo*, we imaged a *Xenopus laevis* (African frog) tadpole. We anesthetized the tadpole and held it partially immersed in water to prevent dehydration and provide index matching. The top part of Fig. 3 shows a conventional ultrahigh-resolution OCT image of an approximately 0.54 mm × 0.5 mm area; we used a bandwidth of 230 nm (center wavelength near 800 nm) to achieve approximately 1 μm × 5 μm (longitudinal × transverse) resolution in the specimen. Tissue morphology as well as pleomorphic mesenchymal cells can be visualized. Cell membranes, cell nuclei, and

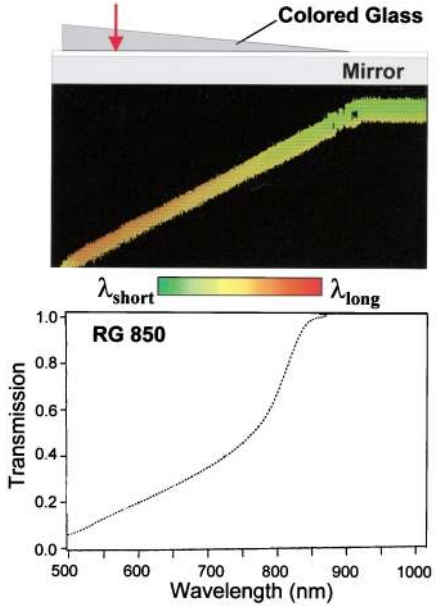

Fig. 2. Spectroscopic OCT image of a colored glass wedge (Schott RG-850) on a silver mirror (top). The colored glass transmission characteristics are depicted on the bottom. In the spectroscopic OCT image a green hue indicates a shift of the spectral center of gravity to shorter wavelengths and a red hue, a shift to longer wavelengths. With increasing wedge thickness, the short-wavelength components of the backreflected spectrum are increasingly absorbed, as can be seen in the variation in hue (green to red) of the mirror reflection.

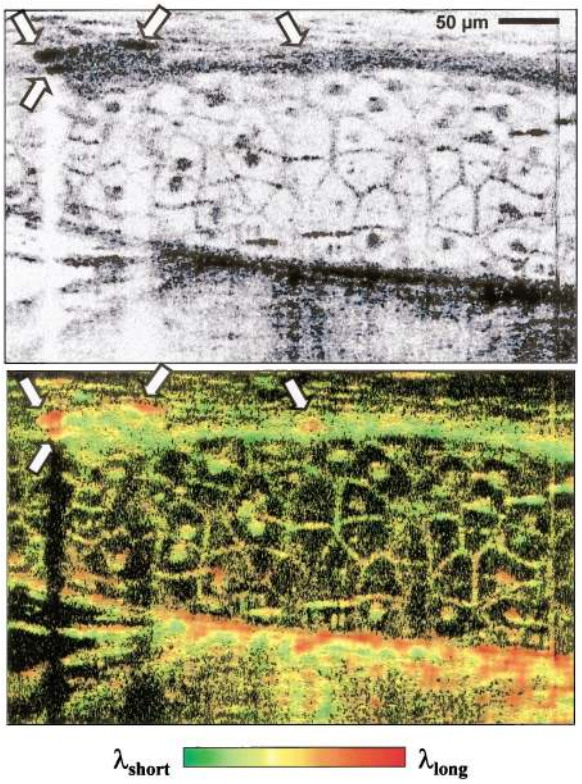

Fig. 3. *In vivo* conventional OCT (approximately 1 μm × 5 μm longitudinal × transverse resolution) and spectroscopic OCT of an African frog tadpole (*Xenopus laevis*). Mesanchymal cells of various sizes are clearly visualized. A green hue indicates a short-wavelength shift of the center of gravity of the spectrum, and a red hue, a long-wavelength shift. Melanocytes (arrows) appear bright red, probably because of enhanced absorption of melanin at shorter wavelengths. Some melanocytes are differentiated by spectroscopic OCT that are difficult to resolve by use of conventional OCT.

melanocytes appear highly backscattering compared with cytoplasm. The bottom part of Fig. 3 shows a spectroscopic OCT image. A red hue indicates a long-wavelength enhancement of the backscattered light, whereas a green hue is a short-wavelength enhancement. The spectroscopic OCT image is consistent with the fact that longer wavelengths penetrate deeper than shorter wavelengths.[12] The shallower structures have a green hue, whereas deeper structures have a red hue. Melanocytes appear bright red in the spectroscopic OCT image, indicating that they are strongly scattering and that they red shift light. The pigmented layer below the cell layer appears red in the spectroscopic OCT image. A melanocyte that is difficult to identify in the conventional OCT image is visible in the upper middle of the image.

It is important to note that OCT image contrast results from a combination of absorption and scattering. Incident light is attenuated by scattering and absorption as it propagates into the tissue, is then backscattered from the internal structure that is being imaged, and is again attenuated as it propagates out of the tissue.[13] Thus, absorption and scattering from deep structures are convolved with the properties of the intervening structures, making it challenging to determine the exact optical properties of a given internal structure. However, OCT provides more information than other spectroscopic imaging techniques that integrate cw backscattered light from multiple tissue depths.

In summary, we have described spectroscopic OCT, which detects and processes the full interferometric signals to provide spatially resolved spectroscopic information. Spectroscopic properties can be measured over the entire bandwidth of the available spectrum in a single measurement. Spectroscopic OCT can enhance image contrast, providing additional information on tissue pathology, and may permit micrometer-scale, cross-sectional, functional imaging of tissue.

We appreciate the contributions of S. A. Boppart and M. Brezinski of the Massachusetts Institute of Technology. U. Morgner and F. X. Kärtner were supported by the Deutsche Forschungsgemeinschaft. W. Drexler was supported by the Max Kade Foundation, Inc., and the Österreichische Akademie der Wissenschaften. This research was supported in part by U.S. Air Force Office of Scientific Research contract F4920-98-1-0139, U.S. Office of Naval Research Medical Free Electron Laser Program contract N000014-97-1-1066, and National Institutes of Health contracts NIH-1-RO1-CA75289-02 and NIH-1-RO1-EY11289-14.

References

1. D. Huang, E. A. Swanson, C. P. Lin, J. S. Schuman, W. G. Stinson, W. Chang, M. R. Hee, T. Flotte, K. Gregory, C. A. Puliafito, and J. G. Fujimoto, Science **254,** 1178 (1991).
2. Z. Chen, T. E. Milner, S. Srinivas, X. Wang, A. Malekafzali, M. J. C. van Gemert, and J. S. Nelson, Opt. Lett. **24,** 1119 (1997).
3. J. A. Izatt, M. D. Kulkami, S. Yazdanfar, J. K. Barton, and A. J. Welch, Opt. Lett. **22,** 1439 (1997).
4. M. R. Hee, D. Huang, E. A. Swanson, and J. G. Fujimoto, J. Opt. Soc. Am. A **9,** 903 (1992).
5. J. F. De Boer, T. E. Milner, M. J. C. van Gemert, and J. S. Nelson, Opt. Lett. **22,** 934 (1997).
6. U. Morgner, F. X. Kärtner, S. H. Cho, Y. Chen, H. A. Haus, J. G. Fujimoto, E. P. Ippen, V. Scheuer, G. Angelow, and T. Tschudi, Opt. Lett. **24,** 411 (1999).
7. W. Drexler, U. Morgner, F. X. Kärtner, C. Pitris, S. A. Boppart, X. D. Li, E. P. Ippen, and J. G. Fujimoto, Opt. Lett. **24,** 1221 (1999).
8. M. D. Kulkarni and J. A. Izatt, in *Conference on Lasers and Electro Optics*, Vol. 9 of 1996 OSA Technical Digest Series (Optical Society of America, Washington, D.C., 1996), pp. 59–60.
9. J. M. Schmitt, S. H. Xiang, and K. M. Yung, J. Opt. Soc. Am. A **15,** 2288 (1998).
10. U. S. Sathyam, B. W. Colston, L. B. DaSilva, and M. J. Everett, Appl. Opt. **38,** 2097 (1999).
11. I. Daubechies, IEEE Trans. Inf. Theory **36,** 961 (1990).
12. P. Parsa, S. L. Jacques, and N. S. Nishioka, Appl. Opt. **28,** 2325 (1989).
13. J. M. Schmitt and A. Knuttel, J. Opt. Soc. Am. A **14,** 1231 (1997).